NASA
Technical
Paper
2528

February 1986

An Approximate Buckling Analysis for Rectangular Orthotropic Plates With Centrally Located Cutouts

Michael P. Nemeth,
Manuel Stein,
and Eric R. Johnson

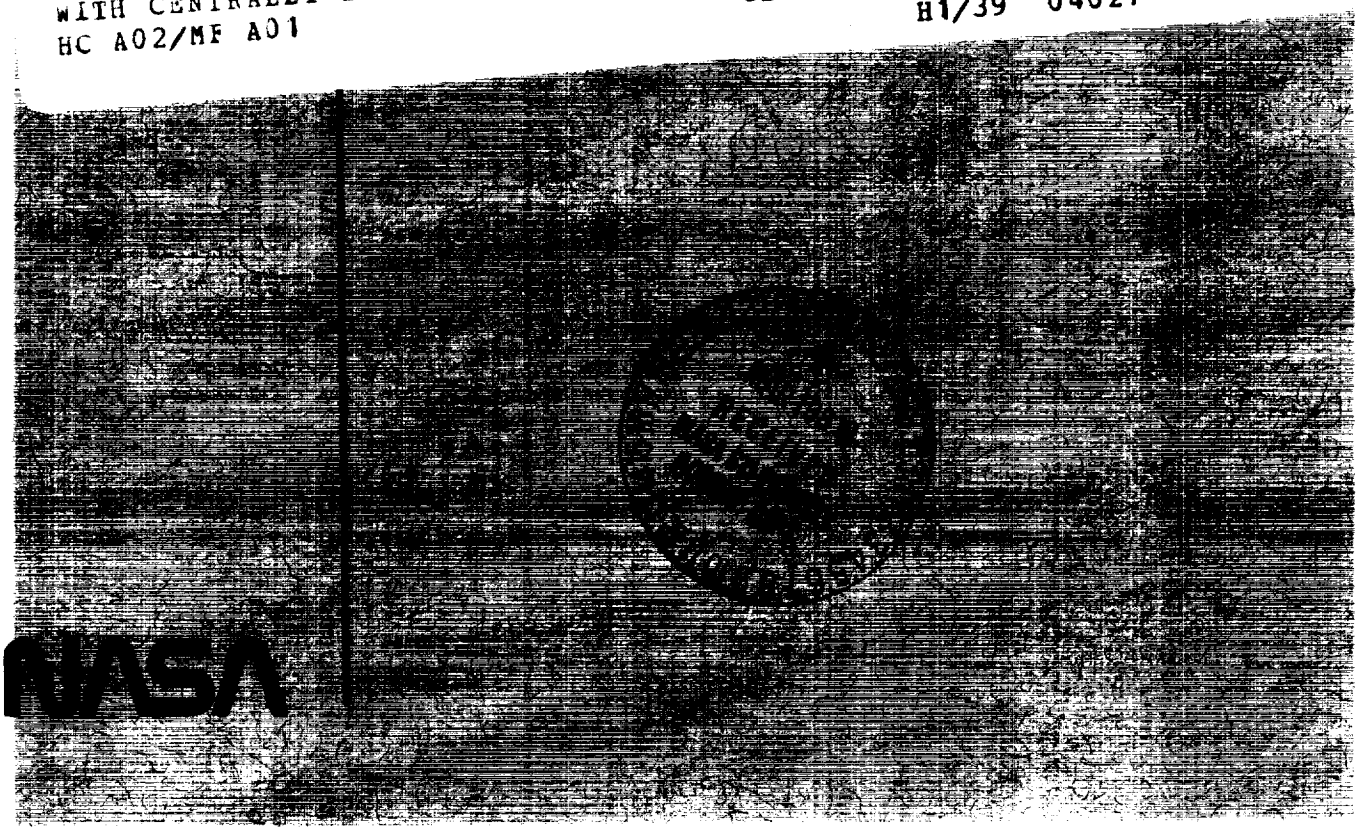

NASA Technical Paper 2528

1986

An Approximate Buckling Analysis for Rectangular Orthotropic Plates With Centrally Located Cutouts

Michael P. Nemeth
and Manuel Stein
Langley Research Center
Hampton, Virginia

Eric R. Johnson
Virginia Polytechnic Institute and State University
Blacksburg, Virginia

National Aeronautics
and Space Administration

Scientific and Technical Information Branch

Abstract

An approximate analysis for predicting buckling of rectangular orthotropic composite plates with centrally located cutouts is presented. In this analysis, the prebuckling and buckling problems are converted from a two-dimensional to a one-dimensional system of linear differential equations with variable coefficients. The conversion is accomplished by expressing the displacements as series with each element containing a trigonometric function of one coordinate and a coefficient that is an arbitrary function of the other coordinate. Ordinary differential equations are then obtained from a variational principle.

Analytical results obtained from the approximate analysis are compared with finite element analyses for isotropic plates and for $[0_{10}]_S$, $[90_{10}]_S$, and $[(0/90)_5]_S$ specially orthotropic plates with central circular cutouts of various sizes. Experimental results for the specially orthotropic plates are also presented. In nearly all cases, the approximate analysis predicts the buckling mode shapes correctly and predicts the buckling loads to within a few percent of the finite element and experimental results.

Introduction

In aircraft and spacecraft structures, cutouts are commonly found as access ports for mechanical and electrical systems. Often during flight, structural members with cutouts experience compression loads, and thus the ability of a compression member with a cutout to resist buckling is important in design. Several studies of the elastic buckling behavior of isotropic square plates containing central circular cutouts have been presented in the technical literature. Reference 1 presents a summary of these studies. Substantially fewer studies (e.g., refs. 1-3) of the elastic buckling behavior of rectangular laminated composite plates with cutouts appear in the technical literature. Understanding the buckling behavior of a rectangular composite plate with a centrally located traction-free cutout provides valuable insight into the behavior of more complicated structural members.

Closed-form solutions for the buckling of plates with finite lengths and widths and with centrally located cutouts are presently beyond the state of the art. Hence, various approximate analyses have been used to study buckling of plates with cutouts. Most of the previous studies have focused on the square plate with a central circular cutout. Before the advent of the finite element method, approximate analyses for performing buckling calculations for these plates typically used boundary collocation methods or the Rayleigh-Ritz method. The major disadvantage of these analyses is the computational difficulty associated with the numerical integration of the potential energy over the doubly connected region, especially in those studies performed before the use of high-speed digital computers became routine. General purpose finite element computer programs, such as EAL (ref. 4), are now available to solve a broad class of plate buckling problems. With proper discretization, accurate solutions can be obtained. However, for a specific problem, a special purpose analysis tailored to the problem characteristics is more appealing than general purpose finite element analyses, in terms of cost, ease of usage, and convenience of parametric studies.

The objective of this paper is to present an approximate analysis that accurately predicts buckling of rectangular specially orthotropic composite plates with centrally located cutouts. The results of this analysis are compared with finite element results and with experimental results. The scope of the analysis presented in this paper includes uniaxial compression loadings, symmetrical cutout shapes, and simply supported and clamped boundary conditions.

Symbols

Although the data are given in both SI and U.S. Customary Units, the measurements and calculations were made in U.S. Customary Units.

$A_{11}, A_{12}, A_{22}, A_{66}$	orthotropic membrane stiffnesses, N/m (lb/in.)
b, c	rectangular plate half-width and half-length (see fig. 1), cm (in.)
d	circular cutout diameter, cm (in.)
$D_{11}, D_{12}, D_{22}, D_{66}$	orthotropic bending stiffnesses, N-m (in-lb)
F	integrand defined by equation (14), J/m (in-lb/in.)
K	nondimensional buckling coefficient given by equation (19)
L	rectangular plate length, equal to 2c (see fig. 1), cm (in.)
N	number of terms in the prebuckling displacement series (see eqs. (2))
N_x, N_y, N_{xy}	membrane stress resultants, N/m (lb/in.)

N_x^{cr}	average N_x stress resultant at buckling, N/m (lb/in.)
N_x^o	N_x stress resultant in a plate without a cutout, N/m (lb/in.)
P_{cr}	buckling load, N (lb)
S	number of terms in the buckling displacement series (see eq. (13))
u, v	prebuckling displacements in the x- and y-directions, respectively, cm (in.)
U_B	bending energy, defined by equation (11), J (in-lb)
U_{IS}	initial stress energy, defined by equation (12), J (in-lb)
U_m	membrane energy, defined by equation (1), J (in-lb)
$\hat{U}_m$	energy integrand defined by equation (3), J/m (in-lb/in.)
u_0, u_{2k-1}, v_{2k-1}	generalized displacements for prebuckling problem, cm (in.)
v_0	displacement series parameter
w	out-of-plane buckling displacement, cm (in.)
W	rectangular plate width, equal to $2b$ (see fig. 1), cm (in.)
W_E	external work defined by equation (4), J (in-lb)
w_{2k-1}	generalized displacements for buckling, cm (in.)
x, y, z	Cartesian coordinates, cm (in.)
$( )'$	differentiation of ( ) with respect to x
δ	variational operator
$\varepsilon_x^o, \varepsilon_y^o, \gamma_{xy}^o$	midplane membrane strains of plate
λ	nondimensional loading parameter defined in equations (2)
$\lambda \tilde{N}_x^0$	applied normal stress resultant, N/m (lb/in.) (see fig. 1)
$\Lambda_0, \Lambda_{2k-1}$	functions defined by equation (5)

Analysis

In this paper, the classical two-dimensional buckling analysis for plates is converted into a simpler approximate one-dimensional analysis following the Kantorovich method (ref. 5, pp. 304–327). The formulation of the present analysis consists of two parts: calculation of the in-plane stress distribution prior to buckling, referred to as the "prebuckling problem," and calculation of the buckling load, referred to as the "buckling problem." In the discussion that follows, the requirements of the approximate analysis are described and the Kantorovich method is applied to obtain the one-dimensional prebuckling and buckling equations.

Plate Description

The formulation of the analysis as a one-dimensional problem implies certain symmetry properties in the geometry, material properties, loading, and boundary conditions. The geometry, loading conditions, and coordinate system used in the analysis are shown in figure 1. The plate has length $L = 2c$, width $W = 2b$, and uniform thickness and is referred to a right-handed Cartesian coordinate system with origin at the center of the plate. The cutouts must be centrally located and must possess shapes that are symmetrical with respect to the xz- and yz-planes. Similarly, the principal orthotropic material axes must coincide with the x- and y-axes of the plates. The loading is applied symmetrically at the $x = \pm c$ edges by either uniformly displacing the two opposite edges of the plate or by applying a uniform normal stress to these edges (see fig. 1). Prior to buckling, the unloaded lateral edges of the plate at $y = \pm b$ are free to expand in-plane in the y-direction. At buckling, these edges are considered simply supported. Only the shaded portion of the plate shown in figure 1 is used to derive the equations in this analysis because of the symmetry discussed previously.

Prebuckling Analysis

Prior to buckling, the potential energy of the plate is the difference between the strain energy due to stretching U_m (also referred to as the "membrane strain energy") and the work done by the external loads W_E.

Exploiting the problem symmetry allows the strain energy prior to buckling to be expressed as

$$U_m = \int_{-c}^{c}\int_{f(x)}^{b}\left[A_{11}(\varepsilon_x^o)^2 + A_{22}(\varepsilon_y^o)^2 + 2A_{12}\varepsilon_x^o\varepsilon_y^o + A_{66}(\gamma_{xy}^o)^2\right] dy\,dx \qquad (1)$$

where $f(x)$ is the curve shown in figure 1, which follows the centerline of the plate and the cutout boundary; A_{ij} are the orthotropic membrane stiffnesses; and $\varepsilon_x^o, \varepsilon_y^o$, and γ_{xy}^o are the linear midplane strains of the two-dimensional theory of elasticity. Following the Kantorovich method, the prebuckling displacements are represented by kinematically admissible series containing products of trigonometric functions of the y-coordinate and generalized displacements that are functions of the x-coordinate. The two major considerations used in this paper to select these series are as follows: (1) the series should adequately approximate the in-plane displacements of the plates and (2) the series should not produce any nonzero resultant forces on the unloaded edges of the plates. These considerations led to selection of the following series to represent the prebuckling displacements of the plates:

$$\left.\begin{aligned} u(x,y) &= \lambda\left\{u_0(x) + \sum_{k=1}^{N} u_{2k-1}(x)\cos\left[(2k-1)\frac{\pi y}{2b}\right]\right\} \\ v(x,y) &= \lambda\left\{v_0 y + \sum_{k=1}^{N} v_{2k-1}(x)\sin\left[(2k-1)\frac{\pi y}{2b}\right]\right\} \end{aligned}\right\} \qquad (2)$$

where λ is a nondimensional loading parameter that is increased monotonically from zero until buckling occurs. The term λu_0 in the series for u and the term $\lambda v_0 y$ in the series for v represent the exact solution for a plate without a cutout. The remaining terms in the series represent corrections to the displacement field that account for the presence of a cutout. The constant v_0 is selected to satisfy the condition that no resultant normal forces act on the unloaded edges of the plate (ref. 1). Substituting the displacement series into the strain-displacement relations of the two-dimensional theory of elasticity, then substituting the resulting expressions into equation (1), and integrating over y yields the membrane strain energy in the following form:

$$U_m = \lambda^2 \int_{-c}^{c} \widehat{U}_m\, dx \qquad (3)$$

where $\widehat{U}_m$ is a function of the generalized displacements u_0, u_{2k-1}, and v_{2k-1} $(k = 1, 2, \ldots, N)$ and their first derivatives with respect to x, that is, u_0', u_{2k-1}', and v_{2k-1}' $(k = 1, 2, \ldots, N)$.

The external work done by the applied loads is given by

$$W_E = -\lambda \tilde{N}_x^o \int_{-b}^{b} [u(c,y) - u(-c,y)]\, dy \qquad (4)$$

where $\lambda\tilde{N}_x^o$ is the applied uniform stress loading shown in figure 1. Substituting the displacement series for $u(x,y)$ given in equations (2) into equation (4) and integrating over y yields the external work in the following form:

$$W_E = -2\lambda^2 \tilde{N}_x^o \left[u_0(x)\Lambda_0(x) + \sum_{k=1}^{N} u_{2k-1}(x)\Lambda_{2k-1}(x)\right]_{x=-c}^{x=+c} \qquad (5)$$

The functions $\Lambda_0(x)$ and $\Lambda_{2k-1}(x)$ are determined directly from integration of the displacement series.

Applying the principle of minimum potential energy results in the following ordinary differential equations and boundary conditions for the prebuckling problem

Differential equations $(-c \le x \le c)$

$$\left.\begin{aligned} \frac{\partial \widehat{U}_m}{\partial u_0} - \frac{d}{dx}\left(\frac{\partial \widehat{U}_m}{\partial u_0'}\right) &= 0 \\ \frac{\partial \widehat{U}_m}{\partial u_{2k-1}} - \frac{d}{dx}\left(\frac{\partial \widehat{U}_m}{\partial u_{2k-1}'}\right) &= 0 \\ \frac{\partial \widehat{U}_m}{\partial v_{2k-1}} - \frac{d}{dx}\left(\frac{\partial \widehat{U}_m}{\partial v_{2k-1}'}\right) &= 0 \end{aligned}\right\} \qquad (6)$$

for $k = 1, 2, 3, \ldots, N$.

Boundary conditions

$$\left.\begin{aligned} \left[\left(\frac{\partial \widehat{U}_m}{\partial u_0'} + \Lambda_0 \tilde{N}_x^o\right)\delta u_0\right]_{x=-c}^{x=+c} &= 0 \\ \left[\left(\frac{\partial \widehat{U}_m}{\partial u_{2k-1}'} + \Lambda_{2k-1}\tilde{N}_x^o\right)\delta u_{2k-1}\right]_{x=-c}^{x=+c} &= 0 \\ \left[\left(\frac{\partial \widehat{U}_m}{\partial v_{2k-1}'}\right)\delta v_{2k-1}\right]_{x=-c}^{x=+c} &= 0 \end{aligned}\right\} \qquad (7)$$

for $k = 1, 2, 3, \ldots, N$.

For the uniform edge-displacement loading, the displacement is prescribed to be a unit displacement times the loading parameter (see fig. 1), and the shear stress resultant is required to vanish at $x = \pm c$, the edges of the plate. Thus, for this loading case,

$$\left.\begin{aligned} u_0(\pm c) &= \mp\frac{1}{2} \\ u_{2k-1}(\pm c) &= 0 \\ v'_{2k-1}(\pm c) - (2k-1)\frac{\pi}{2b}u_{2k-1}(\pm c) &= 0 \end{aligned}\right\} \quad (8)$$

for $k = 1, 2, 3, \ldots, N$. For the uniform edge-stress loading condition, the normal stress resultant is prescribed to be equal to the loading parameter times an arbitrary applied load $\tilde{N}_x^o$, and the shear stress resultant is required to vanish at $x = \pm c$ (see fig. 1). Thus, for this loading case,

$$\left.\begin{aligned} A_{11}u'_0(\pm c) + A_{12}v_0 &= -\tilde{N}_x^0 \\ A_{11}u'_{2k-1}(\pm c) + A_{12}(2k-1)\frac{\pi}{2b}v_{2k-1}(\pm c) &= 0 \\ v'_{2k-1}(\pm c) - (2k-1)\frac{\pi}{2b}u_{2k-1}(\pm c) &= 0 \end{aligned}\right\} \quad (9)$$

for $k = 1, 2, 3, \ldots, N$.

Buckling Analysis

Using the Trefftz criterion, the buckling problem can be posed as

$$\delta(U_B + U_{IS}) = 0 \quad (10)$$

where U_B and U_{IS} are the contributions of the bending energy and the membrane energy (referred to as the "initial stress energy"), respectively, to the second variation of the total potential energy (ref. 1). Exploiting the problem symmetry allows these energies to be expressed as

$$U_B = \int_{-c}^{c}\int_{f(x)}^{b} [D_{11}(w_{,xx})^2 + D_{22}(w_{,yy})^2 + 2D_{12}(w_{,xx}w_{,yy}) + 4D_{66}(w_{,xy})^2]\, dy\, dx \quad (11)$$

and

$$U_{IS} = \int_{-c}^{c}\int_{f(x)}^{b} [N_x(w_{,x})^2 + N_y(w_{,y})^2 + 2N_{xy}w_{,x}w_{,y}]\, dy\, dx \quad (12)$$

where $f(x)$ is the same curve shown in figure 1 and described in the prebuckling analysis section, D_{ij} are the orthotropic bending stiffnesses, N_x, N_y, and N_{xy} are the prebuckling membrane stress resultants, and subscript commas followed by letters denote partial differentiation with respect to the coordinate corresponding to each letter. Both U_B and U_{IS} are derived using the Von Karman nonlinear strain-displacement relations and the principle of minimum potential energy. Following the Kantorovich method, the out-of-plane displacement $w(x, y)$ is approximated by a kinematically admissible trigonometric series given by

$$w(x, y) = \sum_{k=1}^{S} w_{2k-1}(x)\cos\left[(2k-1)\frac{\pi y}{2b}\right] \quad (13)$$

This series also satisfies the natural boundary conditions when the unloaded edges are simply supported.

Substituting the above series expressions for the out-of-plane displacement and the expressions for the prebuckling stress resultants (obtained from solution of eqs. (6)) into equations (11) and (12), and integrating over y yields a functional of the form

$$U_B + U_{IS} = \int_{-c}^{c} F\, dx \quad (14)$$

where F is a function of the generalized displacements w_{2k-1} $(k = 1, 2, 3, \ldots, S)$ and their first and second derivatives with respect to x, w'_{2k-1} and w''_{2k-1} $(k = 1, 2, 3, \ldots, S)$.

Applying equation (10) to this functional leads to the following stability equations and boundary conditions:

Differential equations $(c \le x < c)$

$$\frac{\partial F}{\partial w_{2k-1}} - \frac{d}{dx}\left(\frac{\partial F}{\partial w'_{2k-1}}\right) + \frac{d^2}{dx^2}\left(\frac{\partial F}{\partial w''_{2k-1}}\right) = 0 \quad (15)$$

for $k = 1, 2, 3, \ldots, S$.

Boundary conditions

$$\left.\begin{aligned} \left\{\left[\frac{\partial F}{\partial w'_{2k-1}} - \frac{d}{dx}\left(\frac{\partial F}{\partial w''_{2k-1}}\right)\right]\delta w_{2k-1}\right\}_{x=-c}^{x=+c} &= 0 \\ \left[\left(\frac{\partial F}{\partial w''_{2k-1}}\right)\delta w'_{2k-1}\right]_{x=-c}^{x=+c} &= 0 \end{aligned}\right\} \quad (16)$$

for $k = 1, 2, 3, \ldots, S$.

The boundary conditions for the buckling problem considered in this paper are simply supported

or clamped edges at $x = \pm c$. For simply supported edges, the boundary conditions are

$$\left.\begin{aligned} w_{2k-1}(\pm c) &= 0 \\ w''_{2k-1}(\pm c) &= 0 \end{aligned}\right\} \tag{17}$$

for $k = 1, 2, 3, \ldots, S$. For clamped edges, the boundary conditions are

$$\left.\begin{aligned} w_{2k-1}(\pm c) &= 0 \\ w'_{2k-1}(\pm c) &= 0 \end{aligned}\right\} \tag{18}$$

for $k = 1, 2, 3, \ldots, S$.

Calculation of the Buckling Load

The approximate analyses described in the previous sections for the prebuckling and buckling problems result in two systems of linear ordinary differential equations. The analysis for the prebuckling problem produces $2N + 1$ simultaneous second-order differential equations and $4N + 2$ boundary conditions. Some of the boundary conditions are nonhomogeneous. The analysis for the buckling problem produces S simultaneous fourth-order homogeneous differential equations and $4S$ homogeneous boundary conditions. Together these differential equations and corresponding boundary conditions for the buckling problem constitute an eigenvalue problem for the nondimensional loading parameter λ in equations (2). The smallest nontrivial value of λ corresponds to buckling.

In both the prebuckling and the buckling problems, the ordinary differential equations have variable coefficients that prevent closed-form solutions from being obtained. To obtain solutions, the equations are solved numerically by the finite difference method. Details of the finite difference formulation for the prebuckling analysis corresponding to $N = 3$ and for the buckling analysis corresponding to $S = 3$ are presented in reference 6.

Experiment

The specimens tested in this investigation were fabricated from commercially available 450 K (350°F) cure graphite-epoxy preimpregnated tapes. The tapes were made of unidirectional Hercules AS4 graphite fibers preimpregnated with Hercules 3502 thermosetting epoxy resin. The tapes were laid up to form 20-ply-thick laminates having $[0_{10}]_s$, $[(0/90)_5]_s$, and $[90_{10}]_s$ stacking sequences. The laminates were cured in an autoclave using the manufacturer's recommended procedures. After curing, the laminates were ultrasonically C-scanned to establish specimen quality and then machined into test specimens. All specimens were 25.4 cm (10 in.) long and 25.4 cm (10 in.) wide, and the loaded edges were machined flat and parallel to permit uniform compressive loading. Centrally located circular cutouts were machined into the panels with diamond-impregnated core drills. The hole diameters ranged from 0 to 15.88 cm (6.25 in.). One side of each specimen was painted white to reflect light so that a moiré fringe technique could be used to monitor out-of-plane deformations.

The specimens were loaded in axial compression with a 1.33-MN (300-kip) capacity hydraulic testing machine. The loaded ends of the specimens were clamped by fixtures during testing, and the sides were simply supported by restraints that prevented the specimen from buckling as a wide column. All specimens were loaded slowly to approximately twice the buckling load. A typical specimen mounted in the test fixture is shown in figure 2.

A total of 20 specimens were tested; they were designated A1 through A7 for the $[0_{10}]_s$ specimens, B1 through B6 for the $[90_{10}]_s$ specimens, and C1 through C7 for the $[(0/90)_5]_s$ specimens. The analytical results presented in the results and discussion section of this paper are based on length and width dimensions of 24.13 cm (9.50 in.). These dimensions represent the portion of the plate between edge supports of the test fixture (see fig. 2) that deforms out of plane when buckling occurs. The analytical results are also based on the average value of several thickness measurements made on each specimen. These average thickness values were determined to be 2.718 mm (0.107 in.) for the $[0_{10}]_s$ laminates, 2.692 mm (0.106 in.) for the $[90_{10}]_s$ laminates, and 2.794 mm (0.110 in.) for the $[(0/90)_5]_s$ laminates.

Electrical resistance strain gages were used to monitor strains, and direct-current differential transformers were used to monitor axial displacements and displacements normal to the specimen surface. Electrical signals from the instrumentation and the corresponding applied loads were recorded on magnetic tape at regular time intervals during the tests.

Results and Discussion

Results obtained with the analysis presented in this paper were compared with finite element results and with experimental results to determine the accuracy of the approximate analysis. The converged finite element results were obtained from the computer program EAL (ref. 4). The results for the approximate analyses for $N = 1$ and 2 and $S = 1$ and 2 were obtained from computer programs similar to the computer program described in reference 6.

The computer program described in reference 6 corresponds to the approximate analysis for $N = S = 3$ in equations (2) and (13).

The plates used to assess the accuracy of the approximate analysis were square because square plates exhibit larger differences in the displacement and stress fields for the loading conditions and boundary conditions considered in this paper than do rectangular plates. Previous studies (refs. 1 3) have shown that the buckling load of a simply supported square isotropic plate decreases monotonically with increasing cutout size when a uniform compressive stress is applied to two opposite edges of the plate. When the loading is applied as a uniform compressive displacement of two opposite edges, the buckling load of these plates decreases slightly and then increases with increasing cutout size, until the cutout size becomes larger than approximately 70 percent of the plate width. Rectangular plates with aspect ratios greater than 1 typically exhibit buckling behavior bounded by the buckling behavior for the two loading conditions of the square plates. Hence, square plates are expected to serve as a more rigorous test of the ability of the approximate analysis to predict buckling accurately.

The analytical and experimental results presented in the following sections of this paper are for square plates with centrally located circular cutouts having ratios of diameter to plate width d/W ranging from 0 to 0.66. The influence of orthotropy on the accuracy of the analysis is investigated by studying $[0_{10}]_S$, $[90_{10}]_S$, and $[(0/90)_5]_S$ specially orthotropic laminates. These laminates represent the two extreme cases and one intermediate case of laminate orthotropy.

All results presented in this section are for laminates made of graphite-epoxy plies having longitudinal modulus E_1 of 127.8 GPa (18.5×10^6 psi), transverse modulus E_2 of 11.0 GPa (1.6×10^6 psi), in-plane shear modulus G_{12} of 5.7 GPa (0.832×10^6 psi), and major Poisson's ratio ν_{12} of 0.35. A nominal ply thickness of 0.127 mm (0.005 in.) is used in the analytical comparisons with the finite element analyses.

Analytical Results

Accuracy of the prebuckling analysis. The stress distribution in a plate prior to buckling must be determined in order to determine the plate's buckling load. For plates without cutouts, finding an analytical expression for the prebuckling stress distribution is often trivial. However, for plates with finite dimensions and with a cutout, finding closed-form solutions for the prebuckling stress distribution is presently beyond the state of the art. For the analysis presented herein, the prebuckling stresses are approximated by the truncated displacement series given by equations (2). A highly accurate prebuckling stress analysis may not be needed to predict accurately the buckling load if the overall load distribution in the plate is adequately represented. To assess the applicability of the prebuckling analysis presented in this paper for predicting buckling of plates with cutouts, the N_x and N_y stress resultant distributions at the net section of the plates (located at $x = 0$ in fig. 1) are examined. Results are presented in figures 3 to 8 for both isotropic and specially orthotropic plates. The stress resultant distributions in figures 3 to 8 are normalized by the constant value of N_x in the corresponding plate without a cutout, denoted N_x^o.

In figure 3, the N_x distributions at the plate net section obtained for $N = 1, 2$, and 3 in equations (2) are compared with finite element results for an isotropic plate loaded by uniform edge displacement. The isotropic plate considered in figure 3 has an intermediate ratio of cutout diameter to plate width, $d/W = 0.3$. The results shown in figure 3 indicate that the best approximation to the finite element results is obtained for $N = 3$ (values of N greater than 3 were not considered). Similar results were obtained for two other cutout sizes, $d/W = 0.1$ and 0.6.

The finite element results for $d/W = 0.1$ indicated a stress distribution similar to the stress distribution for a compression-loaded infinite plate with a hole. Most of the plate is uniformly stressed and local stress concentration and gradient are present near the hole. The approximate analysis for $N = 3$ models the uniformly stressed region of the plate very well, but lacks the higher harmonics in the displacement series to give the correct value of the stress concentration near the cutout. An accurate representation of this localized stress concentration may not be required in the prebuckling analysis. The approximate analysis must accurately predict the overall load distribution in the plate, and for $N = 3$, it accomplishes this objective.

The stress distribution for the plate with $d/W = 0.6$ is different from the stress distributions for the plates with $d/W = 0.1$ or 0.3. For this large cutout size, the stress distribution is nonuniform across the entire plate net section without a local stress concentration near the cutout. The results obtained with the approximate analysis suggest that higher harmonics in the displacement series are not required to predict reasonably well the stress distribution in the plate with $d/W = 0.6$. The approximate analysis predicts the overall load distribution in the plates with the larger cutout sizes reasonably well.

The approximate analysis for plates with intermediate cutout sizes is less accurate than the approximate analysis for plates with small or large cutout sizes. Plates with intermediate cutout sizes, such as $d/W = 0.3$, have a large region with a severe stress gradient and a small region with a uniform stress distribution. However, even with the reduced pointwise accuracy of the analysis, the overall load distribution in the plate is adequately represented.

The directional nature of the approximate analysis suggests that orthotropy influences the accuracy of the prebuckling stress predictions. Stress distributions obtained from the finite element analysis and the approximate analysis for $N = 3$, for the displacement-loaded plates, are presented in figures 4 to 7 for the $[0_{10}]_s$ and $[90_{10}]_s$ laminates with $d/W = 0.3$. The results shown in figures 4 to 7 indicate that orthotropy does influence the present analysis. For the N_x distribution at the net section of the plate, the approximate analysis predicts the stress distributions reasonably well, with the results for the $[90_{10}]_s$ laminate (fig. 4) agreeing with the finite element analysis results better than the results for the $[0_{10}]_s$ laminate (fig. 5). For the N_y distribution at the net section of the plate, the results of the approximate analysis for the $[0_{10}]_s$ laminate (fig. 6) agree with the finite element results substantially better than those for the $[90_{10}]_s$ laminate (fig. 7). The approximate analysis results for N_y in the $[90_{10}]_s$ laminates exhibit the largest differences from the finite element results.

Contour plots of the N_x distribution obtained from the finite element analysis and from the approximate analysis for $N = 3$ are shown in figure 8 for a $[90_{10}]_s$ laminate with $d/W = 0.4$ (N_x is normalized by N_x^o). These contour plots suggest that the approximate analysis predicts the overall axial load distribution in the plate reasonably well. Similar results were obtained for N_x, N_y, and N_{xy} distributions for $[0_{10}]_s$ and $[90_{10}]_s$ laminates with $d/W = 0.1$, 0.4, and 0.6. These results also suggest that the approximate analysis adequately predicts the overall load distribution in a plate except for N_y in the $[90_{10}]_s$ laminates with $d/W > 0.3$. The approximate analysis generally predicts the load distributions in the $[90_{10}]_s$ laminates, but not to the same accuracy as for the other laminates.

The results shown in figures 3 to 8 suggest that the approximate prebuckling analysis for $N = 3$ is not suitable for highly accurate stress analysis of plates with cutouts. However, the approximate analysis appears to predict the overall load distribution in the plates reasonably well and may be sufficient for predicting buckling loads.

Accuracy of the buckling analysis. The accuracy of the buckling displacement approximations given by equation (13) is evaluated using $N = 3$ in the prebuckling analysis. Buckling results for displacement-loaded and stress-loaded isotropic square plates with central circular cutouts are shown in figure 9. The plates are simply supported on all edges, and the buckling load is expressed in terms of a nondimensional buckling coefficient given by

$$K = \frac{N_x^{cr} W^2}{\pi^2 \sqrt{D_{11} D_{22}}} \tag{19}$$

For the stress-loaded plates, N_x^{cr} is the critical value of the applied loading. For the displacement-loaded plates, N_x^{cr} is obtained by dividing the total axial load at buckling P_{cr} by the width of the plate. The results presented in figure 9 show a comparison of the buckling coefficients obtained using equation (13) with $S = 1, 2$ and 3 with the corresponding results obtained from finite element analyses. The results in figure 9 show that for both loading cases, the buckling loads converge monotonically from above toward the finite element solutions as the value of S increases. The best agreement between the approximate and finite element analyses is for $S = 3$, with the difference in the buckling coefficients being less than 6 percent for $d/W = 0$, 0.1, 0.2, 0.3, 0.4, and 0.5 and about 10 percent for $d/W = 0.6$. Moreover, the results for the isotropic plates given in table I indicate that both the approximate (for $N = S = 3$) and finite element analyses predict the same buckling mode shapes. The buckling mode shapes consist of a single half-wave along the direction of the applied loading and a single half-wave in the direction perpendicular to the loading.

The influence of orthotropy on the accuracy of the approximate analysis is indicated by the results presented in figure 10 and table I. Approximate results obtained using $N = S = 3$ and finite element results are presented in the figure and in the table for simply supported $[0_{10}]_s$, $[90_{10}]_s$, and $[(0/90)_5]_s$ displacement-loaded laminates with $d/W = 0$ to 0.6. The best agreement between the approximate and finite element results was obtained for the $[0_{10}]_s$ and the $[(0/90)_5]_s$ laminates. The buckling loads from the two analyses for these laminates differed by less than 6 percent for all cutout sizes considered. For the $[90_{10}]_s$ laminates, the difference in the buckling loads increased as d/W increased: the loads for $d/W = 0$, 0.1, and 0.2 differed by less than 2 percent; for $d/W = 0.3$, by slightly less than 8 percent; and for $d/W = 0.4$, 0.5, and 0.6, by 13 to 15 percent. These differences in the buckling loads for $[90_{10}]_s$ laminates with $d/W = 0.4$, 0.5, and 0.6 suggest that this group

of laminates is the most sensitive to the directional nature of the approximate analysis. This sensitivity is manifested in the N_y prebuckling stress prediction.

For all cases presented in table I, with the exception of the $[90_{10}]_s$ laminate with $d/W > 0.2$, the approximate analysis predicts the buckling loads to within 10 percent of the finite element results and predicts the same buckling mode shapes. For the $[90_{10}]_s$ laminate with $d/W \geq 0.3$, the approximate and finite element analyses predict buckling loads that differ by less than 15 percent. However, the approximate analysis for $d/W = 0.3$ predicts a different mode shape from that predicted by the finite element analysis. This incorrect prediction of the mode shape is attributed to the lower accuracy of the N_y prebuckling stress resultant approximation for the $[90_{10}]_s$ laminates, due to the directional nature of the approximate analysis previously discussed.

Experimental Results

The buckling loads obtained for $N = S = 3$ in the approximate analysis are compared with experimental buckling loads for simply supported isotropic plates in reference 1. The cutout sizes range from $d/W = 0$ to 0.6 and results are presented for both uniform edge-stress and uniform edge-displacement loadings. For all cases considered in reference 1, good agreement between the present analysis and the experiments is indicated.

In this study, experimental buckling loads were obtained and compared with the corresponding analytical buckling loads for the $[0_{10}]_s$, $[(0/90)_5]_s$, and $[90_{10}]_s$ laminates previously described to further assess the accuracy of the approximate analysis. The results of this comparison are presented in figure 11 and tables II to IV. The experimental buckling load for each specimen was obtained by determining the value of the applied load at which the slope of the load vs. end-shortening curve changed. A shadow moiré technique for monitoring the out-of-plane displacement was also used to verify the experimental buckling load calculations and to identify the buckling mode shapes. The buckling mode shapes of the plates indicated in tables II to IV consist of either one or two half-waves along the direction of the applied loading. For all the plates, the buckling mode shapes consist of a single half-wave in the direction perpendicular to the loading direction. The experimental and analytical buckling loads shown in figure 11 and listed in tables II to IV agree well except for the $[0_{10}]_s$ laminate with $d/W = 0.6$ and 0.66 and the $[(0/90)_5]_s$ laminate with $d/W = 0.66$. The analytical results for the $[(0/90)_5]_s$ laminates with $d/W \leq 0.6$ and $[0_{10}]_s$ laminates with $d/W < 0.4$ are within 5 percent of the experimental results. The analytical and experimental results for the $[0_{10}]_s$ laminates with $d/W = 0.42$ differ by approximately 12 percent, but with $d/W \geq 0.6$, they differ by more than 25 percent. The agreement between the analytical and experimental results for the $[90_{10}]_s$ laminates is typically not as good as for the other laminates with similar cutout sizes, especially for the smaller cutout sizes, but the differences between the experimental and analytical buckling loads never exceed 13 percent. The analytical buckling load for the $[90_{10}]_s$ laminate with $d/W = 0.66$ was within 3 percent of the experimental buckling load. The $[90_{10}]_s$ laminate designated as specimen B2 in table III buckled into a mode shape that was not predicted by the approximate analysis. The difference between the analytical and experimental buckling loads is approximately 9 percent for this specimen. This result reinforces the previous suggestion that the analysis does not approximate the N_y prebuckling stress resultant for the $[90_{10}]_s$ laminates as well as it does for the other laminates.

The $[0_{10}]_s$ and $[90_{10}]_s$ laminates represent extreme degrees of orthotropy, and the most disagreement between the analytical and experimental buckling loads occurs for these laminates, with the $[90_{10}]_s$ laminates typically showing the worst disagreement overall. This larger disagreement for the $[90_{10}]_s$ laminates is attributed to the lower accuracy of the N_y prebuckling stress resultant predicted by the approximate analysis for the $[90_{10}]_s$ laminates compared with that for the $[0_{10}]_s$ and $[(0/90)_5]_s$ laminates. The buckling loads for the $[(0/90)_5]_s$ laminates (laminates without an extreme degree of orthotropy) are predicted accurately by the approximate analysis for cutout sizes with $d/W \leq 0.6$. In addition, both the experimental and the analytical results for the $[(0/90)_5]_s$ laminates indicate that the buckling load increases as the cutout size increases, as do the results reported by Ritchie and Rhodes (ref. 7) for isotropic plates. This analytical and experimental trend suggests that the buckling resistance of a plate might be improved by optimizing its cutout size as well as its stacking sequence.

Concluding Remarks

An analysis for predicting buckling of rectangular orthotropic composite plates with centrally located cutouts has been presented. In this analysis, the prebuckling and buckling problems are converted into systems of linear ordinary differential equations with variable coefficients. The conversion is accomplished by expressing the displacements as series with each element containing a trigonometric function of one coordinate and a coefficient that is an arbitrary

function of the other coordinate. Ordinary differential equations are then obtained from a variational principle.

Buckling loads obtained from the approximate analysis are compared with buckling loads obtained from finite element analyses for isotropic plates and for $[0_{10}]_s$, $[90_{10}]_s$, and $[(0/90)_5]_s$ specially orthotropic plates. The plates contain central circular cutouts having diameters d ranging in sizes from 0 to nearly 70 percent of the plate width ($0 \leq d/W \leq 0.66$). Experimental results are also presented for the specially orthotropic laminates.

The comparison of the approximate and finite element results suggests that a highly accurate pointwise prebuckling stress analysis is not essential for accurately predicting the buckling load, as long as the prebuckling stress analysis gives the general load distribution in the plate. The comparison also indicates that in most cases the approximate analysis predicts the buckling loads to within 10 percent of the buckling loads obtained from a finite element analysis. Orthotropy plays an important role in the accuracy of the approximate analysis (with regard to the directional dependence associated with the choice of the displacement series) and is most important in the analysis of the $[90_{10}]_s$ laminates. For the $[90_{10}]_s$ laminates with $d/W > 0.3$, the approximate analysis predicts the overall prebuckling load distribution with less accuracy than for the other laminates and results in differences from 13 percent to 15 percent in the buckling loads obtained by the approximate and finite element analyses. For the $[0_{10}]_s$ and $[(0/90)_5]_s$ specially orthotropic plates and isotropic plates, the differences between the buckling loads obtained from the approximate analysis and the buckling loads obtained from the finite element analysis are at most 10 percent for cutout sizes with $d/W \leq 0.6$.

Experimental results presented indicate that the approximate analysis predicts buckling loads to within 13-percent accuracy in most cases. Specifically, the approximate analysis predicts buckling of the $[(0/90)_5]_s$ laminates to within 5 percent of the experimentally obtained buckling load for cutout sizes up to $d/W = 0.6$. Similar accuracy in the buckling load predictions was obtained for the $[0_{10}]_s$ laminates with cutout sizes up to $d/W < 0.4$. The approximate analysis results for the $[0_{10}]_s$ laminates with $d/W = 0.6$ and 0.66 and for the $[(0/90)_5]_s$ laminates with $d/W = 0.66$ differed from the experimental results by more than 25 percent. The buckling load obtained from the approximate analysis for the $[90_{10}]_s$ laminate with $d/W = 0.66$ was within 3 percent of the experimental buckling load. Both the analytical and the experimental results presented in this paper indicated that increasing the cutout size in a given plate does not always reduce the buckling load.

NASA Langley Research Center
Hampton, VA 23665-5225
October 30, 1985

References

1. Nemeth, Michael Paul: Buckling Behavior of Orthotropic Composite Plates With Centrally Located Cutouts. Ph.D. Diss., Virginia Polytech. Inst. & State Univ., May 1983.
2. Martin, James: Buckling and Postbuckling of Laminated Composite Square Plates With Reinforced Central Circular Holes. Ph.D. Diss., Case Western Reserve Univ., 1972.
3. Preobrazhenskii, I. N.: Research Pertaining to Stability of Thin Plates With Holes. *Soviet Appl. Mech.*, vol. 16, no. 7, Jan. 1981, pp. 557–574.
4. Whetstone, W. D.: EISI-EAL Engineering Analysis Language Reference Manual EISI-EAL System Level 2091. Engineering Information Systems, Inc., July 1983.
5. Kantorovich, L. V.; and Krylov, V. I. (Curtis D. Benster, transl.): *Approximate Methods of Higher Analysis.* Interscience Pub., Inc., c.1964.
6. Nemeth, Michael P.: *A Buckling Analysis for Rectangular Orthotropic Plates With Centrally Located Cutouts.* NASA TM-86263, 1984.
7. Ritchie, D.; and Rhodes, J.: Buckling and Post-Buckling Behavior of Plates With Holes. *Aeronaut. Q.*, vol. 26, pt. 4, Nov. 1975, pp. 281–296.

TABLE I. BUCKLING COEFFICIENTS FOR SIMPLY SUPPORTED DISPLACEMENT-LOADED SQUARE PLATES OBTAINED FROM THE APPROXIMATE AND FINITE ELEMENT ANALYSES

[All plates buckled into one half-wave in each coordinate direction unless otherwise noted]

Ratio of cutout diameter to plate width, d/W	$[90_{10}]_s$			$[0_{10}]_s$			$[(0/90)_5]_s$			Isotropic		
	Approx. analysis	Finite element analysis	Difference,[a] percent	Approx. analysis	Finite element analysis	Difference,[a] percent	Approx. analysis	Finite element analysis	Difference,[a] percent	Approx. analysis	Finite element analysis	Difference,[a] percent
0	[b]2.84	[b]2.84	0	4.50	4.51	0.2	2.46	2.46	0	4.00	4.00	0
0.1	[b]2.86	[b]2.90	1.4	4.37	4.33	−.9	2.39	2.36	−1.3	3.93	3.86	−1.8
.2	[b]2.98	[b]3.01	1.0	3.92	3.96	1.0	2.19	2.14	−2.3	3.69	3.59	−2.8
.3	[b]3.12	2.90	−7.6	3.62	3.66	1.1	2.01	1.96	−2.6	3.51	3.43	−2.3
.4	3.10	2.71	−14.4	3.45	3.44	−.3	1.91	1.84	−3.8	3.58	3.47	−3.2
.5	2.99	2.63	−13.7	3.36	3.32	−1.2	1.87	1.81	−3.3	3.97	3.75	−5.9
.6	3.03	2.67	−13.5	3.48	3.32	−4.8	1.96	1.86	−5.4	4.79	4.36	−9.9

[a] Difference from finite element result.

[b] Mode shape consists of two half-waves in the axial direction and one half-wave in the other direction.

TABLE II. EXPERIMENTAL AND ANALYTICAL BUCKLING LOADS FOR CLAMPED $[0_{10}]_s$ LAMINATES

[All plates buckled into one half-wave in each coordinate direction]

Specimen	Ratio of cutout diameter to plate width, d/W	Cutout diameter, cm (in.)	Buckling Loads, kN (lb)		Difference,[a] percent
			Experiment	Analysis	
A1	0	0 (0)	37.392 (8406)	37.894 (8519)	−1.3
A2	0.11	2.54 (1.00)	36.289 (8158)	36.395 (8182)	−.3
A3	.21	5.08 (2.00)	33.642 (7563)	33.744 (7586)	−.3
A4	.32	7.62 (3.00)	32.530 (7313)	33.958 (7634)	−4.4
A5	.42	10.16 (4.00)	28.455 (6397)	32.041 (7203)	−12.6
A6	.60	14.48 (5.70)	28.638 (6438)	20.916 (4702)	27.0
A7	.66	15.88 (6.25)	27.245 (6125)	3.309 (744)	87.9

[a]Difference from experiment.

TABLE III. EXPERIMENTAL AND ANALYTICAL BUCKLING LOADS FOR CLAMPED $[90_{10}]_s$ LAMINATES

[All plates buckled into one half-wave in each coordinate direction unless otherwise noted]

Specimen	Ratio of cutout diameter to plate width, d/W	Cutout diameter, cm (in.)	Buckling Loads, kN (lb)		Difference,[a] percent
			Experiment	Analysis	
B1	0	0 (0)	[b]9.710 (2183)	[b]9.822 (2208)	−1.2
B2	0.11	2.54 (1.00)	[b]10.889 (2448)	9.937 (2234)	8.7
B3	.21	5.08 (2.00)	8.803 (1979)	8.879 (1996)	−.9
B4	.32	7.62 (3.00)	7.322 (1646)	8.220 (1848)	−12.3
B5	.42	10.16 (4.00)	7.024 (1579)	7.873 (1770)	−12.1
B6	.66	15.88 (6.75)	8.256 (1856)	8.016 (1802)	2.9

[a]Difference from experiment.
[b]Mode shape consists of two half-waves in the axial direction and one in the other direction.

TABLE IV. EXPERIMENTAL AND ANALYTICAL BUCKLING LOAD FOR CLAMPED $[(0/90)_5]_s$ LAMINATES

[All plates buckled into one half-wave in each coordinate direction unless otherwise noted]

Specimen	Ratio of cutout diameter to plate width, d/W	Cutout diameter, cm (in.)	Buckling Loads, kN (lb)		Difference,[a] percent
			Experiment	Analysis	
C1	0	0 (0)	28.842 (6484)	29.087 (6539)	−0.9
C2	0.11	2.54 (1.00)	27.681 (6223)	27.979 (6290)	−1.1
C3	.21	5.08 (2.00)	25.777 (5795)	25.862 (5814)	−.3
C4	.32	7.62 (3.00)	25.880 (5818)	26.391 (5933)	−2.0
C5	.42	10.16 (4.00)	27.610 (6207)	27.348 (6148)	1.0
C6	.60	14.48 (5.70)	27.339 (6146)	26.467 (5950)	3.2
C7	.66	15.88 (6.25)	29.207 (6566)	[b]7.042 (1583)	75.9

[a]Difference from experiment.
[b]Mode shape consists of two half-waves in the axial direction and one in the other direction.

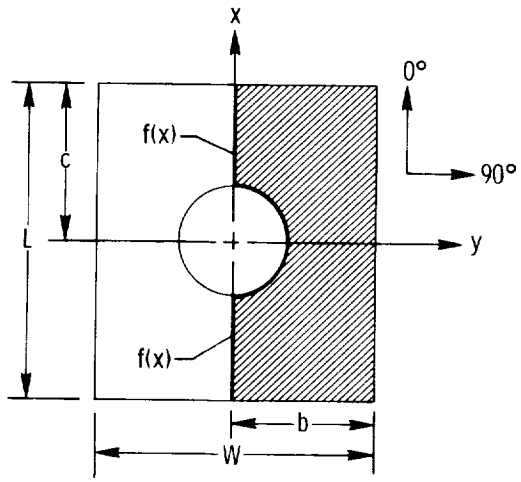

(a) Geometry and coordinate system.

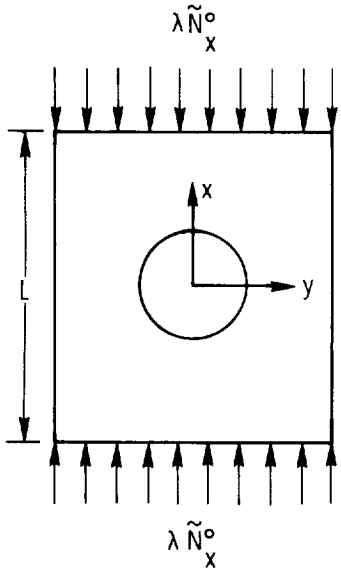

(b) Uniform compressive edge stress.

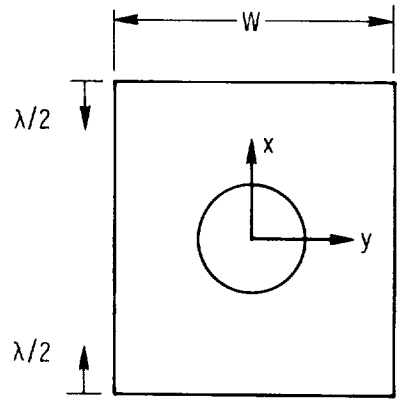

(c) Uniform compressive edge displacement.

Figure 1. Geometry, coordinate system, and loading conditions for rectangular plate with centrally located cutout.

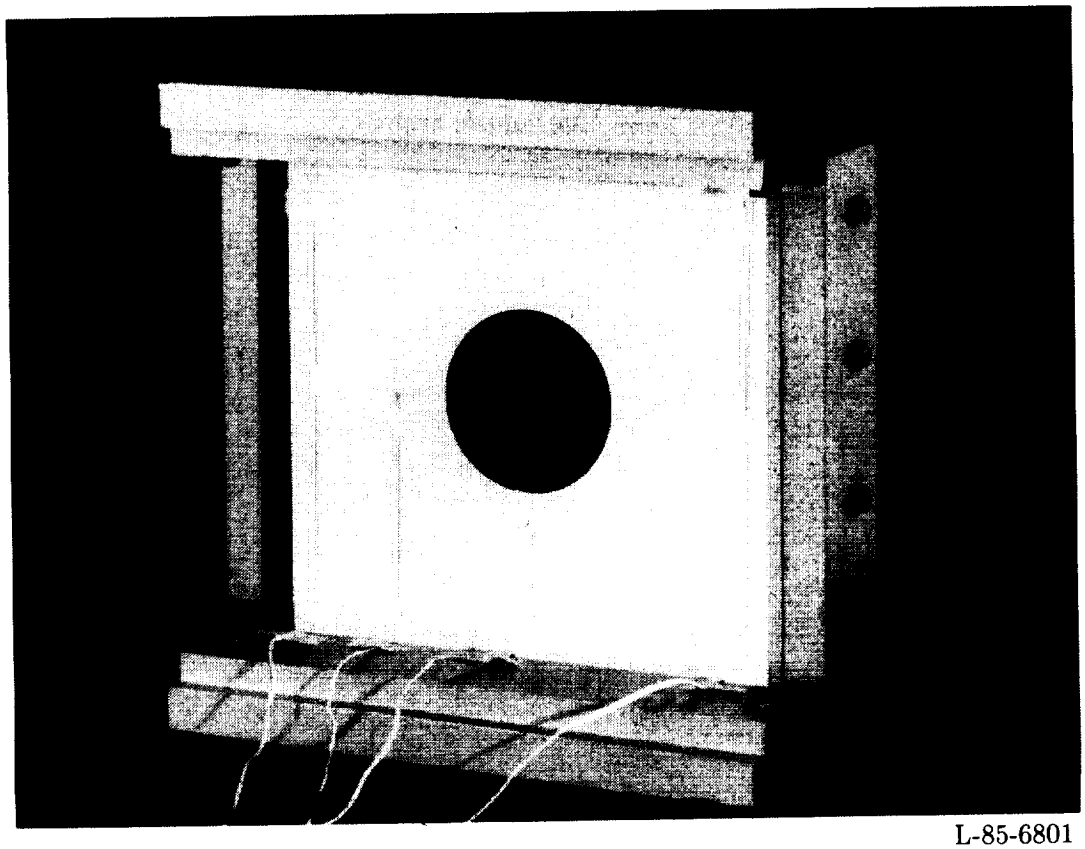

L-85-6801

Figure 2. Specimen mounted in test fixture.

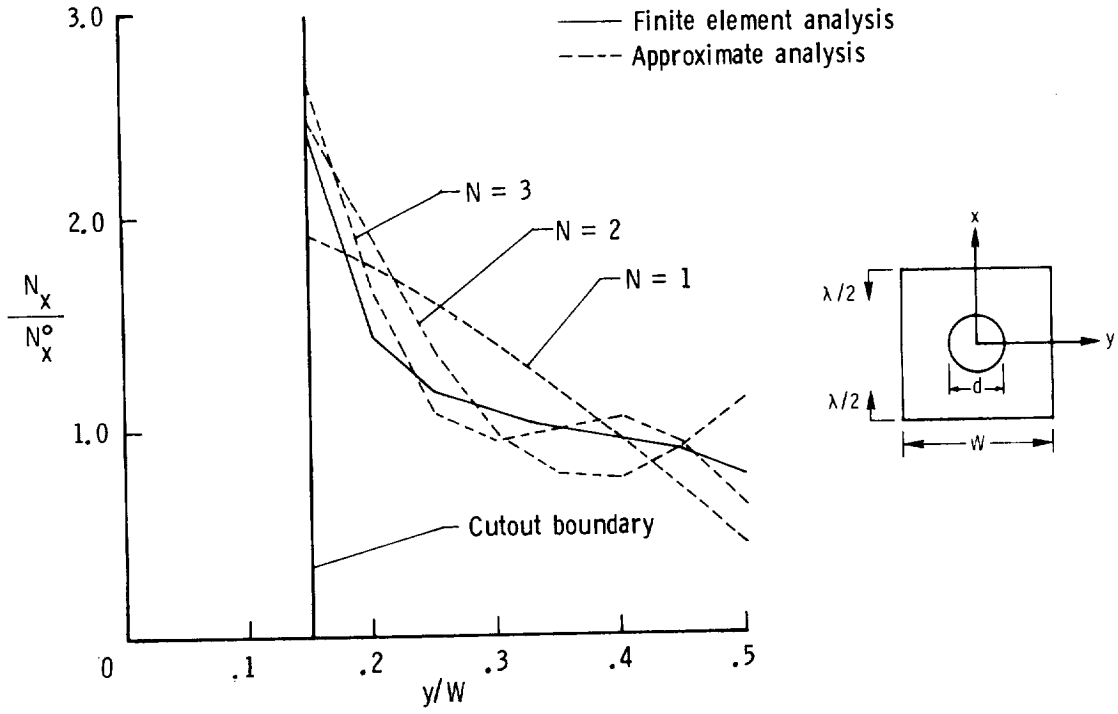

Figure 3. Comparison of the approximate and finite element N_x prebuckling stress distributions at $x = 0$ for a displacement-loaded isotropic plate. $d/W = 0.3$.

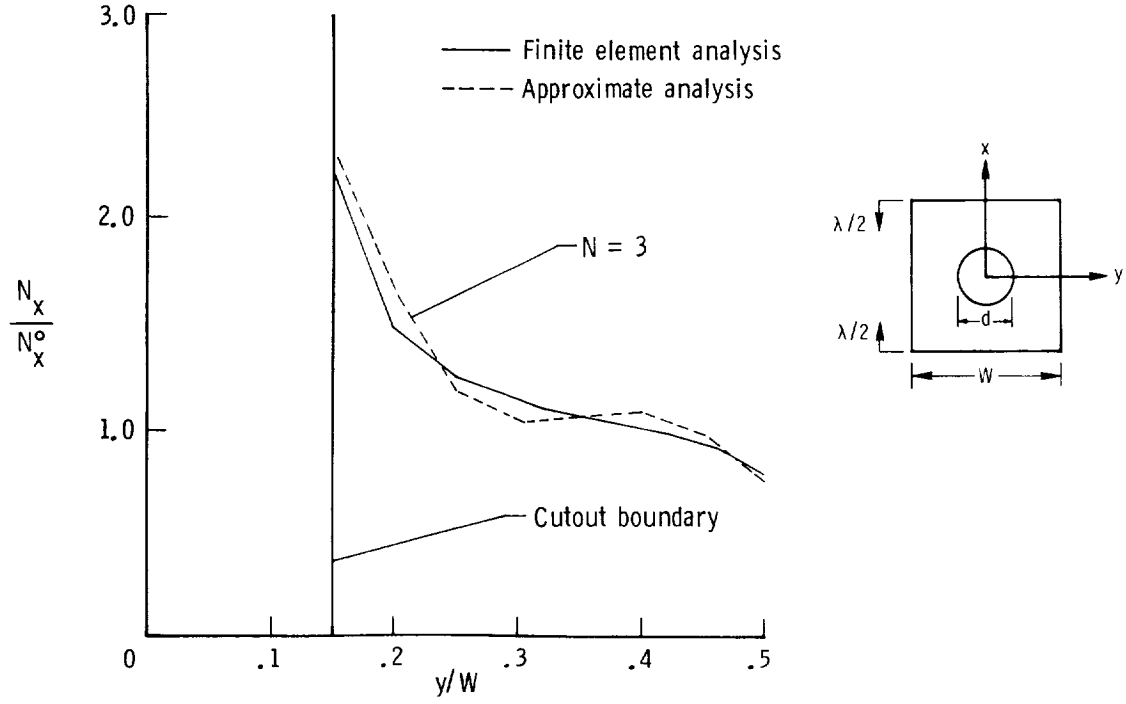

Figure 4. Comparison of the approximate and finite element N_x prebuckling stress distributions at $x = 0$ for a displacement-loaded $[90_{10}]_s$ laminate. $d/W = 0.3$.

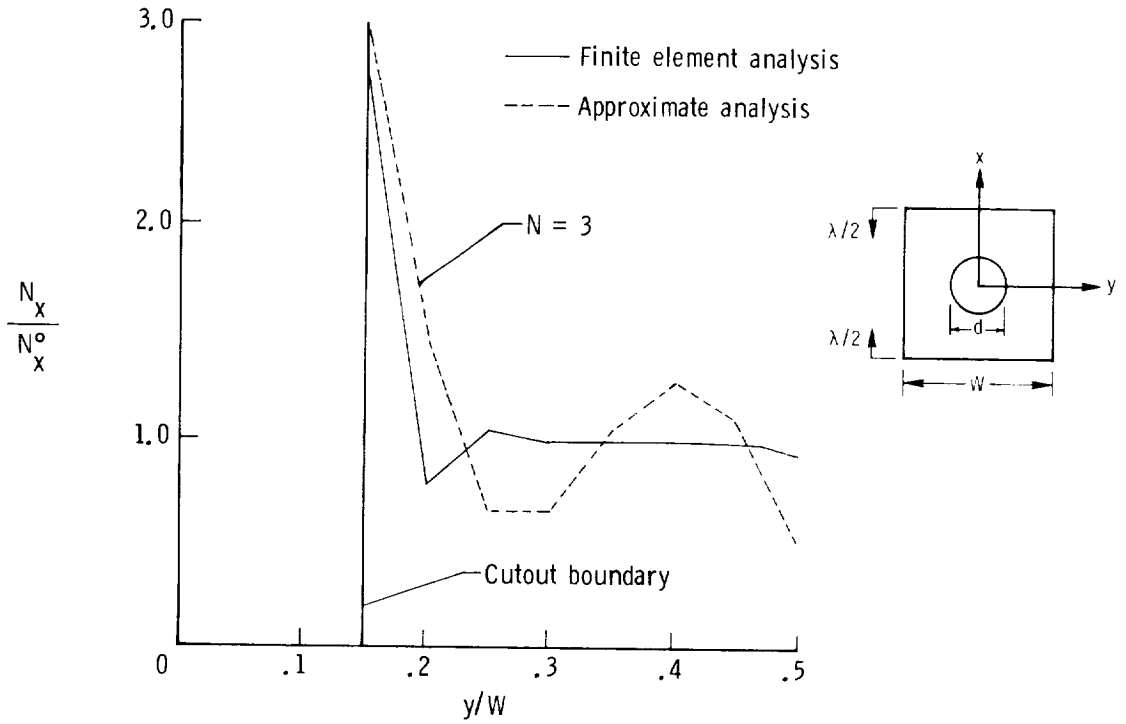

Figure 5. Comparison of the approximate and finite element N_x prebuckling stress distributions at $x = 0$ for a displacement-loaded $[0_{10}]_s$ laminate. $d/W = 0.3$.

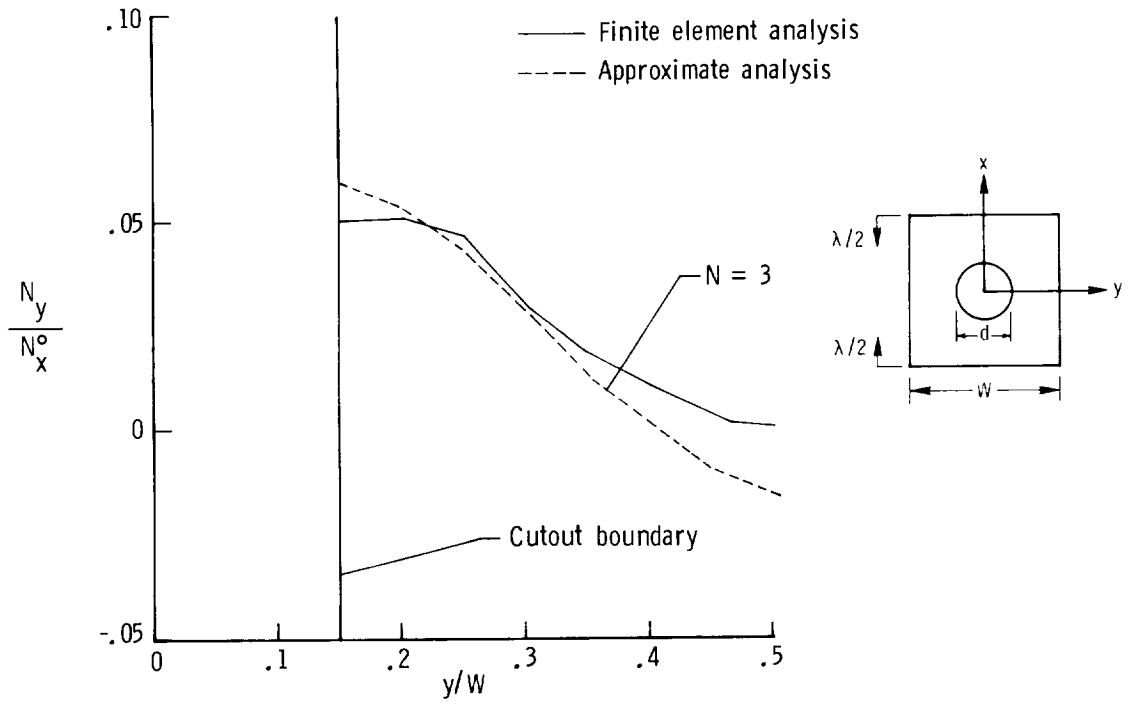

Figure 6. Comparison of the approximate and finite element N_y prebuckling stress distributions at $x = 0$ for a displacement-loaded $[0_{10}]_s$ laminate. $d/W = 0.3$.

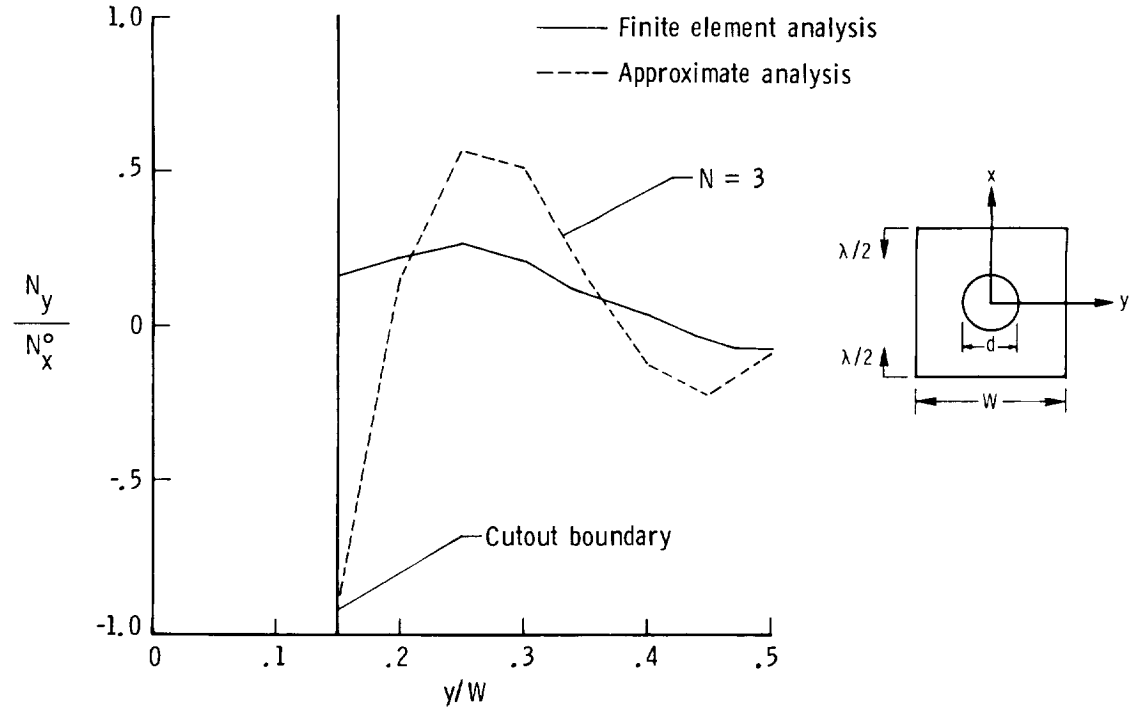

Figure 7. Comparison of the approximate and finite element N_y prebuckling stress distributions at $x = 0$ for a displacement-loaded $[90_{10}]_s$ laminate. $d/W = 0.3$.

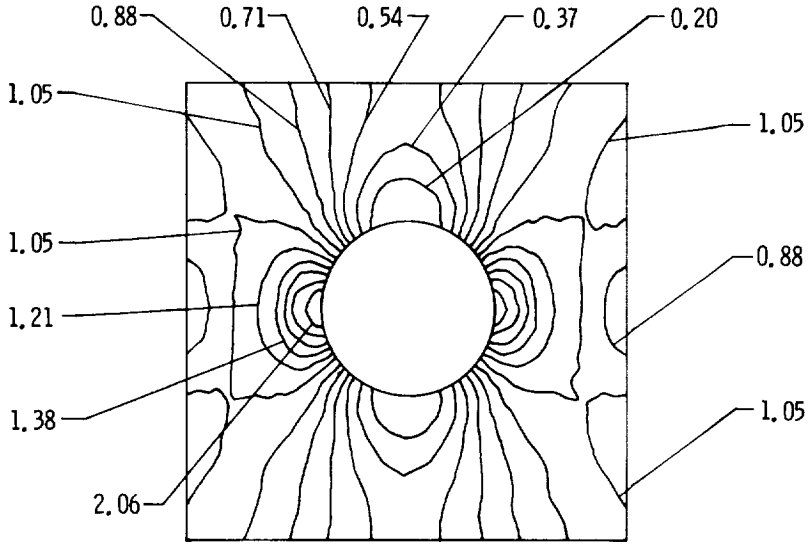

(a) Finite element analysis.

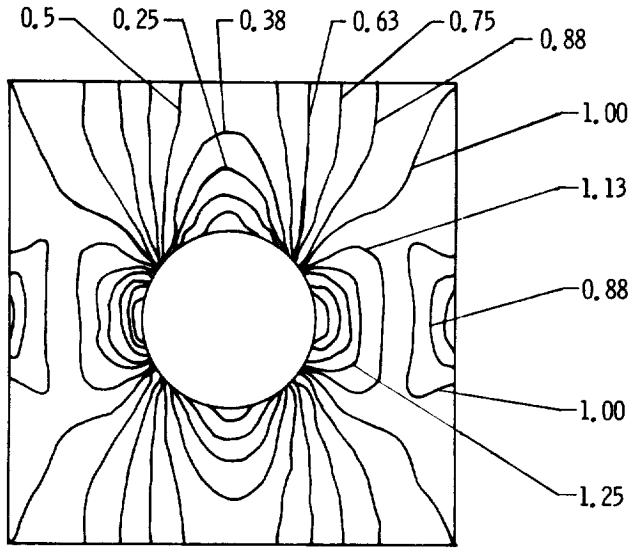

(b) Approximate analysis.

Figure 8. Comparison of the approximate and finite element N_x/N_x^o prebuckling stress resultant contours for the displacement-loaded $[90_{10}]_s$ laminate. $d/W = 0.4$.

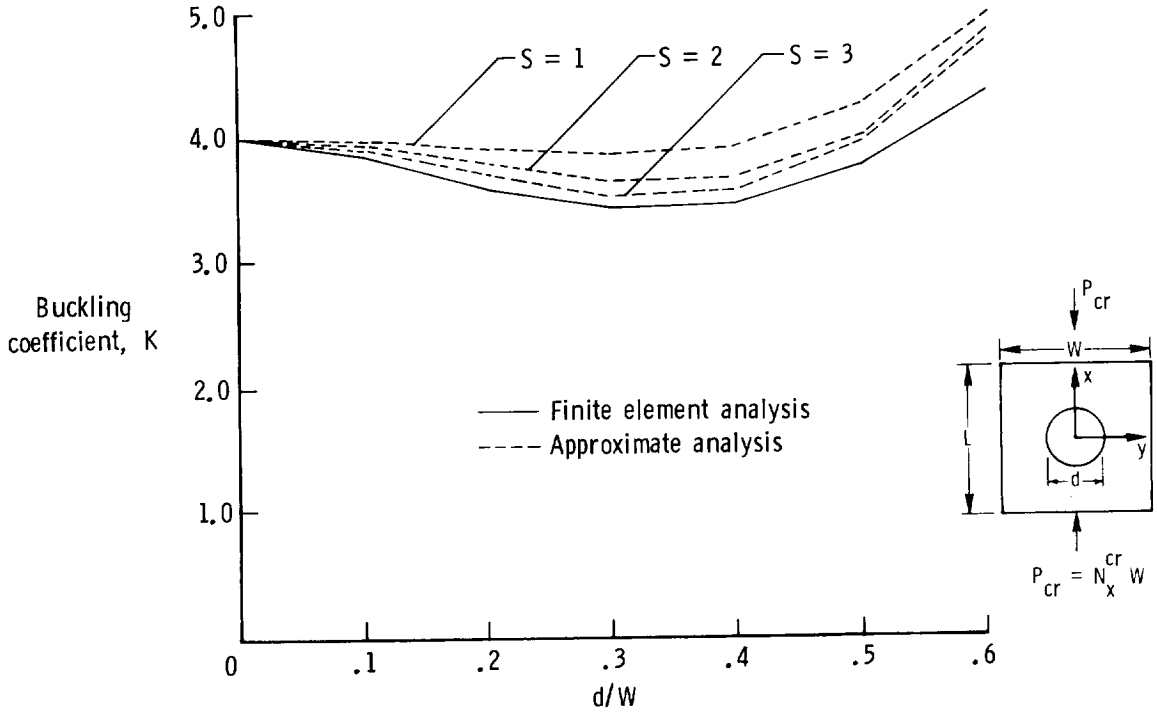

(a) Displacement loading.

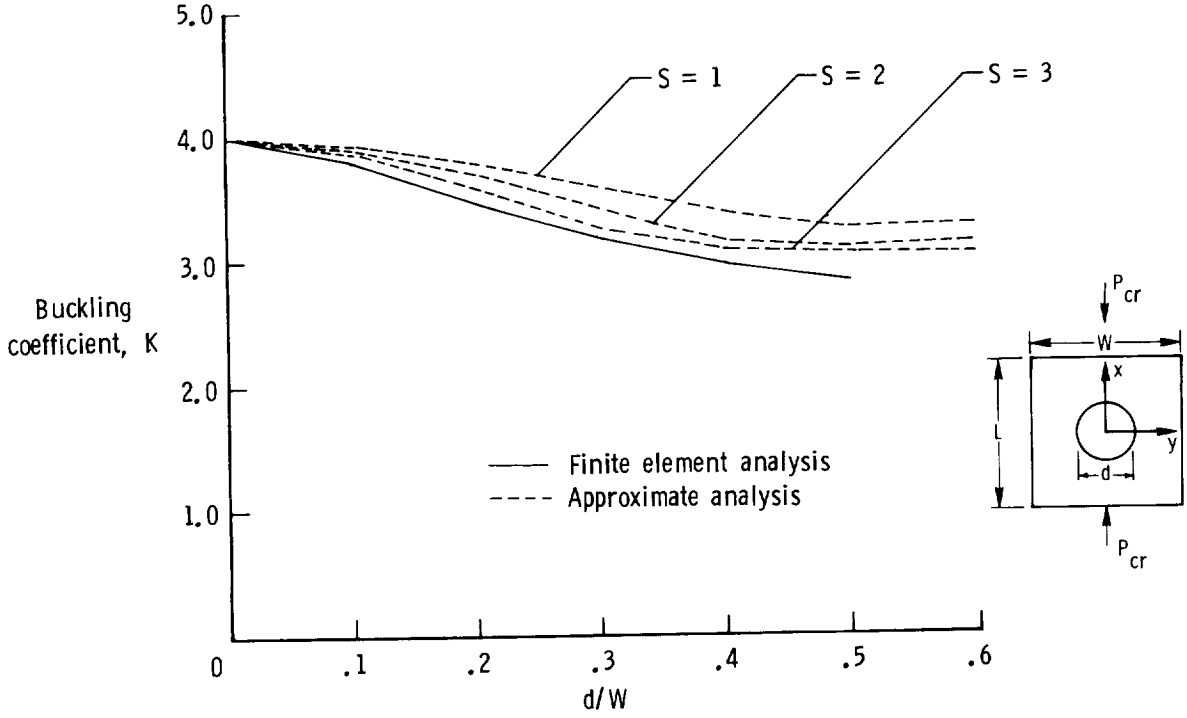

(b) Stress loading.

Figure 9. Comparison of the approximate and finite element buckling coefficients for square simply supported isotropic plates.

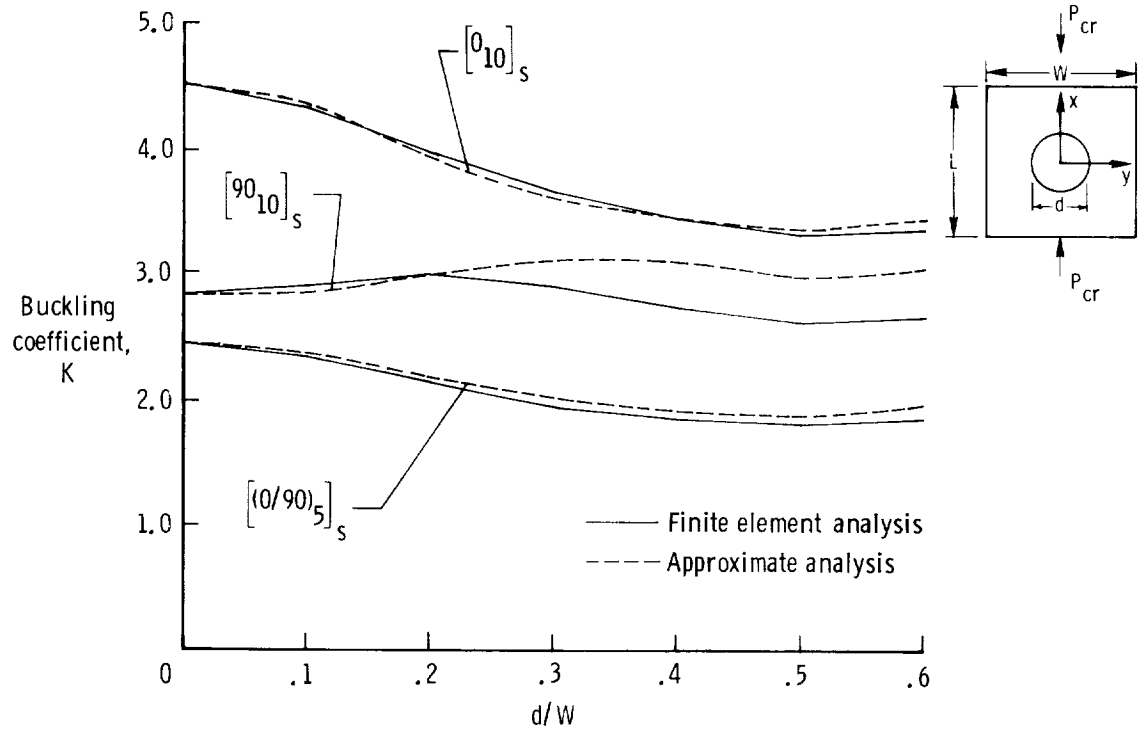

Figure 10. Comparison of the approximate and finite element buckling coefficients for the displacement-loaded $[0_{10}]_s$, $[(0/90)_5]_s$, and $[90_{10}]_s$ simply supported laminates. $N = S = 3$.

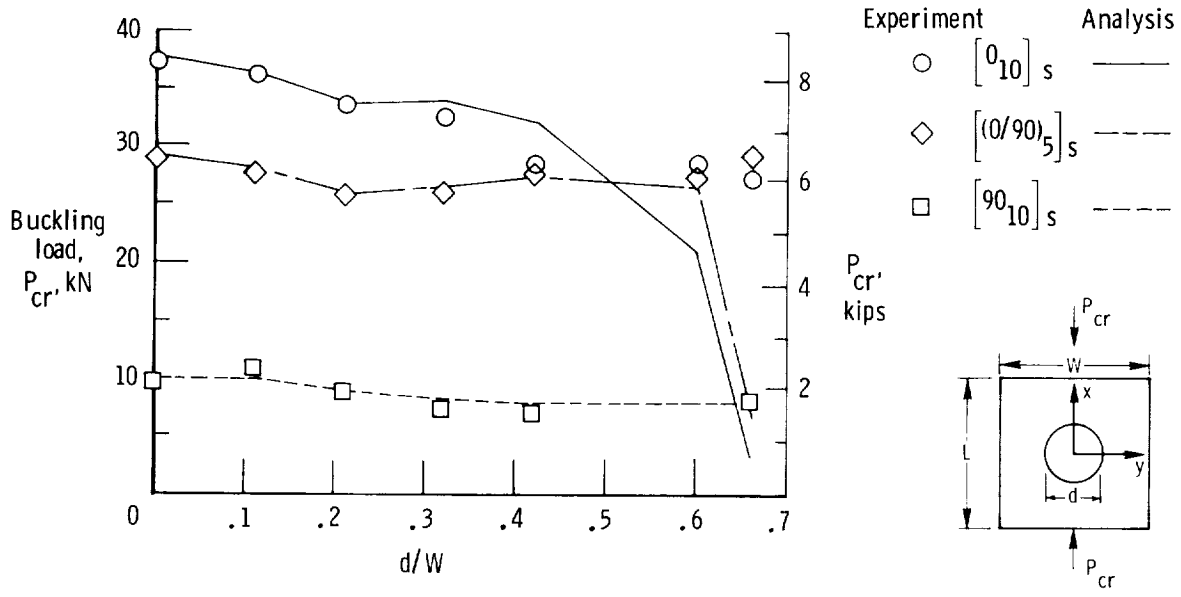

Figure 11. Experimental and approximate buckling loads for clamped specially orthotropic laminates.

1. Report No. NASA TP-2528	2. Government Accession No.	3. Recipient's Catalog No.
4. Title and Subtitle An Approximate Buckling Analysis for Rectangular Orthotropic Plates With Centrally Located Cutouts		5. Report Date February 1986
		6. Performing Organization Code 505-33-33-06
7. Author(s) Michael P. Nemeth, Manuel Stein, and Eric R. Johnson		8. Performing Organization Report No. L-16032
9. Performing Organization Name and Address NASA Langley Research Center Hampton, VA 23665-5225		10. Work Unit No.
		11. Contract or Grant No.
12. Sponsoring Agency Name and Address National Aeronautics and Space Administration Washington, DC 20546-0001		13. Type of Report and Period Covered Technical Paper
		14. Sponsoring Agency Code

15. Supplementary Notes

Michael P. Nemeth and Manuel Stein: NASA Langley Research Center, Hampton, Virginia.
Eric R. Johnson: Virginia Polytechnic Institute and State University, Blacksburg, Virginia.

16. Abstract

An approximate analysis for predicting buckling of rectangular orthotropic composite plates with centrally located cutouts is presented. In this analysis, the prebuckling and buckling problems are converted from a two-dimensional to a one-dimensional system of linear differential equations with variable coefficients. The conversion is accomplished by expressing the displacements as series with each element containing a trigonometric function of one coordinate and a coefficient that is an arbitrary function of the other coordinate. Ordinary differential equations are then obtained from a variational principle. Analytical results obtained from the approximate analysis are compared with finite element analyses for isotropic plates and for $[0_{10}]_S$, $[90_{10}]_S$, and $[(0/90)_5]_S$ specially orthotropic plates with central circular cutouts of various sizes. Experimental results for the specially orthotropic plates are also presented. In nearly all cases, the approximate analysis predicts the buckling mode shapes correctly and predicts the buckling loads to within a few percent of the finite element and experimental results.

17. Key Words (Suggested by Authors(s))	18. Distribution Statement
Plates with cutouts Buckling analysis Kantorovich method	Unclassified - Unlimited Subject Category 39

19. Security Classif.(of this report)	20. Security Classif.(of this page)	21. No. of Pages	22. Price
Unclassified	Unclassified	19	A02

For sale by the National Technical Information Service, Springfield, Virginia 22161 NASA-Langley, 1986